

1 The polymorphism of *Hydra* microsatellite
2 sequences provides strain-specific signatures

3

4 Quentin Schenkelaars^{#a}, Diego Perez-Cortez, Chrystelle Perruchoud and Brigitte Galliot*

5

6 Department of Genetics and Evolution, Institute of Genetics and Genomics in Geneva (iGE3),
7 University of Geneva, Geneva, Switzerland

8

9 * Corresponding author : brigitte.galliot@unige.ch

10

11 ^{#a} Current address: Jacques Monod Institute, Paris, France

12

13

14

15 **Key words:**

16 *Hydra vulgaris* strains, macerate extract, microsatellite polymorphism, PCR barcoding, cryptic

17 species, speciation

18

19 **ABSTRACT**

20 *Hydra* are freshwater polyps widely studied for their amazing regenerative capacity, adult
21 stem cell populations, low senescence and value as ecotoxicological marker. Many wild-type
22 strains of *H. vulgaris* have been collected worldwide and maintained effectively under
23 laboratory conditions by asexual reproduction, while stable transgenic lines have been
24 continuously produced since 2006. Efforts are now needed to ensure the genetic
25 characterization of all these strains, which despite similar morphologies, show significant
26 variability in their response to gene expression silencing procedures, pharmacological
27 treatments or environmental conditions. Here, we established a rapid and reliable procedure
28 at the single polyp level to produce via PCR amplification of three distinct microsatellite
29 sequences molecular signatures that clearly distinguish between *Hydra* strains and species.
30 The TG-rich region of an uncharacterized gene (*ms-c25145*) helps to distinguish between
31 Eurasian *H. vulgaris* strains (*Hm-105*, *Basel1*, *Basel2* and *reg-16*), between Eurasian and North
32 American *H. vulgaris* strains (*H. carnea*, *AEP*), and between the *H. vulgaris* and *H. oligactis*
33 species. The AT-rich microsatellite sequences located in the *AIP* gene (*Aryl Hydrocarbon*
34 *Receptor Interaction Protein*, *ms-AIP*) also differ between Eurasian and North American *H.*
35 *vulgaris* strains. Finally, the AT-rich microsatellite located in the *Myb-Like cyclin D-binding*
36 *transcription factor1* gene (*ms-DMTF1*) gene helps to distinguish certain transgenic *AEP* lines.
37 This study shows that the analysis of microsatellite sequences provides a barcoding tool that
38 is sensitive and robust for the identification of *Hydra* strains. It is also capable of identifying
39 cryptic species by tracing microevolutionary events within the genus *Hydra*.

40

41 INTRODUCTION

42 Since the initial discovery of *Hydra* regeneration by Abraham Trembley in 1744 (1), the
43 freshwater *Hydra* polyp is used as a fruitful model system not only in cell and developmental
44 biology but also for aging, neurobiology, immunology, evolutionary biology and ecotoxicology
45 studies (2–8). *Hydra*, which belongs to Cnidaria, the sister phylum of bilaterians (Fig 1A), is
46 closely related to jellyfish although displaying a life cycle restricted to the polyp stage (Fig 1B).
47 Over the past 100 years, numerous strains were captured all over the world to explore the
48 variability of the *Hydra* genus and the genetic basis of developmental mechanisms (9–11).

49 The analysis of morphological and cellular criteria identified in *Hydra* strains collected
50 worldwide established four distinct groups named *H. oligactis* (stalked *Hydra*), *H. vulgaris*
51 (common *Hydra*), *H. viridissima* (symbiotic green *Hydra*) and *H. braueri* (gracile *Hydra*) (11)
52 (Fig 1B, 1C). The main cellular criterion was provided by the morphology of nematocysts (the
53 venom capsules located inside the mature stinging cells named nematocytes or cnidocytes)
54 that varies between the *Hydra* groups (12). More recently, a series of mitochondrial and
55 nuclear molecular markers were used for barcoding analysis (13–16), which confirmed the
56 relevance of these four groups but also revealed that each group may actually contain several
57 species, e.g. *H. carnea* and formal *H. vulgaris*, also called *H. vulgaris-1*, within the *H. vulgaris*
58 group (Fig 1A).

59 **Fig 1. Phylogenetic position and morphology of the freshwater *Hydra* polyp.**

60 (A) Phylogenetic tree showing the four *Hydra* species among the *Hydra* genus: *H. vulgaris* and
61 *H. carnea* (blue background), *H. oligactis*, *H. braueri*, and *H. viridissima*. (B) Anatomy of *Hydra*,
62 here a *H. viridissima* polyp from the Nicolet strain. *Hydra* polyps exhibit a 0.5-2 cm long tubular
63 structure terminated by the basal disc at the aboral pole and the head at the oral pole. The
64 head region includes a dome structure called the hypostome, terminated by the mouth
65 opening at the tip and surrounded by tentacles at its base. In the lower part of the body

66 column, below the budding zone, the peduncle region precedes the basal disc. Scale bar: 1
67 mm. (C) Morphologies of the *H. vulgaris*, *H. carnea* and *H. oligactis* strains. Note the presence
68 of a stalk peduncle in *H. oligactis* strains. Scale bars : 2 mm.

69

70 Among the formal *H. vulgaris* species, the *H. magnipapillata* strain 105 (*Hm-105*) is a Japanese
71 strain described by Ito in 1947 (17) and widely used since then (9,14). Several European *H.*
72 *vulgaris* strains (*Basel*, *Zürich*, etc.) were also characterized (12), actually found closely related
73 to the Asian *Hm-105* strain. The *AEP* strain, which constitutively produces gametes, was
74 obtained by crossing two North American strains, most likely the *H. carnea* and *H. littoralis*
75 strains, both members of the *H. carnea* species (18,16), subsequently selected for
76 transgenesis (19). Nowadays, the laboratories that use *Hydra* as an experimental model
77 maintain clonal cultures of *H. vulgaris* (*Hm-105*, *Basel*, *Zürich*, *reg-16* strains), but also from *H.*
78 *carnea* (*AEP* strains), *H. viridissima* (e.g. *Nicolet* as Geneva strain) or *H. oligactis* species
79 (*Ho_CS*, *Ho_CR* as European strains) (Fig 1B, 1C). A facility located in Mishima (Japan)
80 maintains for the scientific community specimens from a large variety of strains and species
81 (molevo.sakura.ne.jp/Hydra/magni.html).

82 The importance of identifying the various *Hydra* strains/species relies on the fact that they
83 can exhibit (i) different developmental behaviors, especially the morphogenetic variants that
84 show distinct budding rate or size features in homeostatic context (20–23), (ii) lower
85 regeneration potential such as the *reg-16* strain (24), (iii) abnormal apical patterning such as
86 multiheaded strains (25,26), (iv) specific cellular properties such as the *nf-1* strain that
87 contains neither interstitial stem cells nor interstitial derivatives (27) or the *sf-1* thermo-
88 sensitive strain that loses its cycling interstitial cells upon transient heat-shock exposure (28).
89 Importantly, strains that do not show obvious differences at the morphological or cellular
90 levels actually exhibit variable responses to gene silencing upon RNA interference (29), to drug

91 treatment (30–32) or to environmental stresses (32). In addition, experimental evidences
 92 indicate that strain-specific signals regulate the proliferation of interstitial cells (33).
 93 During the past ten years, efforts were made to obtain the *H. vulgaris* genome (34), reference
 94 transcriptomes and proteomes (35–37), quantitative RNA-seq in homeostatic and
 95 regenerative conditions (38–41) and single-cell transcriptomes (42). Two strains of *H. oligactis*,
 96 one undergoing aging (*Ho_CS*) and the other not (*Ho_CR*) were used for transcriptomic and
 97 proteomic analysis (32), while genomic sequences were made available for the *H. oligactis*
 98 and *H. viridissima* species (41) (See **Table-1**). The current molecular barcoding in *Hydra* is
 99 precise and efficient but time-consuming and relatively costly as based on DNA extractions,
 100 PCRs amplification followed by DNA sequencing, therefore not well-adapted to large-scale
 101 characterization of individual polyps.

Species	Strains	“Omics” analyses in <i>Hydra</i>	Refs -web portals
<i>H. vulgaris-1</i>	<i>Hm-105</i>	- Genome (2010), <i>Hydra 2.0</i> genome (2015) - Whole <i>Hydra</i> Trinity transcriptome (2014) - Regeneration transcriptomics: apical (70%) (2015) - Regeneration Proteomics: apical (70%) (2015) - Single-cell transcriptomics (2019)	(34) NHGRI <i>Hydra</i> (38) NHGRI <i>Hydra</i> (37) (37) (42) NHGRI <i>Hydra</i>
	<i>Basel1</i>	- Reference transcriptome (2013)	(35,36) EBI, Uniprot
	<i>Jussy</i> (Geneva)	- Spatial transcriptomics (2019) - 5 positions along the body column – - Regeneration transcriptomics (2019) - apical (80%, 50%) and basal (50%) -	(40) (41) HydrATLAS (39) (41) HydrATLAS
<i>H. carnea</i> <i>AEP</i> transgenic lines	<i>ecto-GFP; endo-GFP; cnnos-GFP</i>	- Transcriptomics of GFP stem cell populations sorted by flow cytometry (2012, 2016)	(43) Compagen (40) HydrATLAS
	<i>ecto-RFP/endo-GFP; i-cell-RFP</i>	- Transcriptomics of RFP and GFP sorted cells (2014)	(38) NHGRI <i>Hydra</i>
<i>H. oligactis</i>	<i>Ho-CR</i> <i>Ho_CS</i>	- Genomics from <i>Ho_CR</i> (2019) - Transcriptomics on cold-exposed <i>Ho_CR</i> , cold-induced aging <i>Ho_CS</i> (2020) - Proteomics on cold-induced aging ± rapamycin treatment (2020)	(41) HydrATLAS (32) HydrATLAS (32) HydrATLAS
	<i>H. viridissima</i>	<i>Nicolet</i> (Geneva)	- Genomics from <i>Nicolet</i> (2019)

102 **Table-1 : Omics resources in *Hydra*.**

103 See **Table-S3** for details and URLs to access the Compagen, EBI, HydrATLAS, NHGRI *Hydra* web portals.

104

105 Microsatellites consist in tandem repeats of short nucleotide motifs of variable length, e.g.
106 (TA)_n, (CA/TG)_n, (CG)_n, (CAG)_n, where n represent the number of repetitions (44). These
107 microsatellites are distributed at different locations in the genome, and the number of repeats
108 within a given microsatellite may differ between animals of the same species or population.
109 As a result, microsatellites are widely used for DNA profiling in population genetics studies,
110 but also in criminal investigations, paternity testing, or identification of individuals in the event
111 of a mass disaster (45,46). In these studies, individuals with the same number of repeats at a
112 given genomic location are considered to be closely related, while each additional repeat
113 reflects a divergent step. The combined analysis of different microsatellites makes it possible
114 to construct a genotypic fingerprint specific to each individual, which provides accurate
115 information for tracing evolutionary events such as population bottleneck, migrations,
116 expansions, etc.

117 The objective of this work was to establish a rapid, inexpensive and reliable method to
118 characterize animals of each strain used in the laboratory. To this end, we established a
119 method that relies on PCR amplification of microsatellite sequences on a single polyp without
120 DNA extraction or sequencing. We show that the analysis of microsatellite polymorphism in
121 animals from either various wild-type strains or transgenic lines provides specific signatures
122 that reliably distinguish strains of the *H. vulgaris* group. This barcoding method, now routinely
123 applied in our laboratory, is efficient and well suited for large-scale studies.

124 **Materials and Methods**

125 ***Hydra strain collection.***

126 The wild-type strains used in this study were a kind gift from colleagues, *Basel1* and *AEP1* from
127 B. Hobmayer (University of Innsbruck), *Basel2*, *Hm-105* and *Ho_CR* from T. Holstein (University
128 of Heidelberg), *AEP2* from R. Steele (University of California), *Ho_CS* from H. Shimizu (National
129 Institute of Genetics, Mishima) and *Nicolet* from Mr. Nicolet (Geneva). The AEP transgenic
130 lines that constitutively express GFP in their epithelial cells, either gastrodermal (*endo-GFP*)
131 or epidermal (*ecto-GFP*), were produced by the Bosch Lab (University of Kiel) (19,47) (Wittlieb
132 et al., 2006, Anton-Erxleben et al., 2009) and kindly provided to us. The *AEP1* transgenic lines
133 expressing the *HyWnt3-2149::GFP* construct (here named *Wnt3::GFP*) either in epidermal or
134 gastrodermal epithelial cells were produced in-house with the *HyWnt3-2149::GFP-*
135 *HyAct:dsRed* reporter construct kindly given by T. Holstein (48,49). We also produced in the
136 *AEP2* strain the Q82-203 and Q82-293 lines by injecting early embryos with the *HyActin:Q82-*
137 *eGFP* construct (QS, unpublished) following the original procedure (19). All cultures were fed
138 three times a week with freshly hatched *Artemia* and washed with *Hydra* Medium (HM) (24)
139 (Sugiyama and Fujisawa, 1977a).

140 ***One-step preparation of macerate extracts***

141 Polyps were washed three times five minutes in distilled water. Then, single polyps were
142 dissociated into 50 μ L distilled water by energetically pipetting them up and down until there
143 is no tissue left, and immediately transferred on ice. Cell density of each macerate was
144 estimated by measuring the OD₆₀₀ using a NanoDrop One (Thermo Scientific). The DNA content
145 and DNA purity were roughly estimated by measuring the absorbance of each sample at 230,
146 260 and 280 nm. To implement an efficient one-step PCR procedure, we selected three *AEP2*
147 polyps showing a regular size (about 4-6 mm long without the tentacles).

148 ***PCR amplification from macerate extracts***

149 To test the efficiency of PCR amplification on macerate extracts, we used primers of the β -
150 *actin* gene ([Table-S1](#)) on 0, 0.5, 1.5, 5 and 15 μ L macerate extract as template for a final 25 μ L
151 PCR mix (1x Taq Buffer, 1x Coral Load, 400 nM of each primer, 160 nM dNTPs and 0.5 unit of
152 Top Taq Polymerase, Qiagen). Subsequently we used 5 μ L out of 50 μ L macerate extract to
153 amplify the mitochondrial *cytochrome C oxidase I (COI)* gene, the mitochondrial *16S ribosomal*
154 *DNA (16S)* and the microsatellite regions (ms) in each strain ([Table-S1](#)). After an initial
155 denaturation step at 94°C for two minutes, samples were submitted to 30 cycles of (i)
156 denaturation at 94°C for 15 seconds, (ii) annealing at 52°C for 30 seconds and (iii) a 30-60
157 seconds elongation step at 72°C. The process was terminated by a final extension at 72°C for
158 15 minutes. 10 μ L PCR products were run on a 2.5% agarose gel at 120 V for two to three
159 hours in the case of microsatellites, stained with ethidium bromide and revealed under UV-
160 light.

161 ***Cloning and sequencing***

162 For sequence validation, the PCR products were cloned using the pGEMT kit (Promega): 3 μ L
163 PCR products were ligated to 50 ng pGEMT vector in the presence of 3 units T4 ligase overnight
164 at 18°C (final volume 10 μ L). Plasmidic DNA was integrated into competent DH5 α *E. coli* and
165 colonies were screened thanks to alpha-complementation. After overnight culture, plasmidic
166 DNA was extracted using the CTAB procedure and sequenced using standard T7 primer at
167 Microsynth (Basel, Switzerland). The number of colonies we sequenced and their origin (single
168 or several animals) is indicated for each microsatellite sequence in [Table-S3](#).

169 ***Phylogenetic analyses***

170 The *COI* and *16S* genes were selected for phylogenetic analyses. Corresponding DNA
171 sequences were amplified by direct PCR amplification method as described above and
172 sequenced (**Table-S2**). The obtained sequenced were aligned with the dataset previously
173 produced by Martinez et al. (15) using the ClustalW function of BioEdit v7.2.6.1, and Maximum
174 Likelihood phylogenetic trees were constructed with the PhyML 3.0 software
175 (<http://www.atgc-montpellier.fr/phyml/>) applying the GTR substitution model (50). The
176 robustness of the nodes was tested by 1000 bootstraps.

177 **RESULTS**

178 ***One-step genomic amplification after quick mechanical tissue maceration***

179 To bypass genomic and mitochondrial DNA extractions that are time-consuming and
180 expensive when massively performed, we established a rapid animal dissociation in water that
181 provides genomic DNA of sufficient quantity and quality for PCR reaction. Although the
182 efficiency of such PCRs certainly varies with the gene of interest, the primers and the size of
183 the amplicon, we obtained PCRs using macerate extracts resulted in strong bands for *β-actin*
184 (193 bp), implying that the application of a mechanical force to dissociate the tissues and the
185 denaturation step at the beginning of the PCR are sufficient to release high quality genomic
186 DNA to allow the amplification of the target sequence (**Fig 2A**). More precisely, despite slight
187 variations in band intensity, certainly reflecting the amount of starting material, the
188 amplification remained highly efficient whatever the polyp and the template volume used
189 here. Accordingly, for all subsequent experiments, we used one tenth of macerate extract as
190 template for *COI*, *16S* and microsatellite amplifications (**Fig 2B**). We also obtained efficient
191 PCR amplification from macerate extracts prepared from fixed animals stored at -20°C for

192 several years, especially for mitochondrial DNA amplification. This procedure thus allows us
193 to gain genetic information from fresh as well as old samples.

194

195 **Fig 2. Direct genomic DNA amplification from single *Hydra* polyp**

196 **(A)** Efficacy of PCR amplification of β -actin genomic DNA according to the original size of the
197 dissociated polyp. DNA from each polyp was resuspended in 50 μ l. Scale: 2 mm. **(B)** Graphic
198 representation of DNA extraction efficiency and DNA purity as deduced from OD
199 measurements at 260, 230 and 280 nm wave lengths. Each dot represents a value obtained
200 from a single polyp. For each DNA, the efficiency of PCR amplification is indicated with a color
201 code.

202 **Phylogenetic assignation of *Hydra* strains to the different groups and species**

203 Next, we confirmed the assignation of each strain we acquired to one of the four *Hydra* groups
204 previously described (i.e. *H. vulgaris*, *H. oligactis*, *H. viridissima*, *H. braueri*), and when relevant
205 to the species identified within each group, namely *H. vulgaris 1* and *H. carnea* within the *H.*
206 *vulgaris* group (13–16). Briefly, we performed phylogenetic analyses of the *COI* and *16S*
207 sequences, efficiently amplified from one single polyp per strain of interest (*AEP1*, *AEP2*,
208 *Basel1*, *Basel2*, *Hm-105*, *reg-16*, *Ho-CR*, *Ho-CS*, *Nicolet*) as detailed above. The global topology
209 of the *COI* tree retrieves the four orthologous groups (**Fig 3**), which is not the case in the *16S*
210 analysis where the *H. vulgaris* group actually includes the *H. braueri* and *H. oligactis* groups
211 that thus do not appear monophyletic (**Fig S1**).

212 However, in both analyses, the sequences of the strains tested were grouped as expected
213 within the 13 species previously identified (i.e. *H. circumcincta 1 and 2*, *H. hymanae*, *H.*
214 *utahensis*, *H. oligactis*, *H. canadensis*, *H. oxycnida*, *H. carnea* and *H. vulgaris 1 to 5*). The *Hm-*
215 *105* and *Hv_Basel* sequences are grouped in the *H. vulgaris 1* group, a Eurasian group which
216 contains the *Hm-105* reference sequences (GU722892.1 for *COI* and GU722807.1 for *16S*), the
217 *Ho_CS* and *Ho_CR* sequences both belong to the *H. oligactis* group, and the *Nicolet* sequences

218 belong to the *H. viridissima* group. This analysis also confirms that the *AEP* sequences (*AEP1*,
219 *AEP2*) belong to the *H. carnea* group that contains all the sequences of the North American
220 strains of the *H. vulgaris* group and only these sequences (**Fig 3**). We found that the genomic
221 *16S* sequences of the two *Hv_Basel* strains are identical, while the mitochondrial *COI*
222 sequences are different with nine out of 657 bp mismatches (sequences obtained twice
223 independently). Consequently, animals of these two cultures can be considered as belonging
224 to two different strains, which we have named *Basel1* and *Basel2*. In contrast, the *COI* and *16S*
225 sequences of *AEP1* and *AEP2* were identical, suggesting that they could represent a single
226 strain.

227

228 **FIG 3: Phylogenetic relationships within the *Hydra* genus based on the analysis of the**
229 ***Cytochrome Oxidase I (COI) DNA sequences***

230 The maximum likelihood tree of the *COI* sequences was built by adding to the dataset of 85
231 *COI* sequences available on Genbank (15) the 10 sequences obtained in the present study
232 (written in red, see **Table-S3** for accession numbers). Black dots indicate the robustness of the
233 nodes as deduced from the bootstrap support (at least 750 over 1'000 bootstraps). This tree
234 confirms the presence of four distinct *Hydra* groups (*H. viridissima*, *H. braueri*, *H. oligactis* and
235 *H. vulgaris*). Within the *H. vulgaris* group, note the position of the *AEP* sequences within the
236 *H. carnea* sub-group.

237

238 ***Identification of three microsatellite regions in the *Hydra* genome***

239 We then analyzed some microsatellite sequences to test the conclusions obtained in the
240 phylogenetic analyses and to establish a method for easy identification of strains belonging to
241 the *H. vulgaris* group. To identify *H. vulgaris* genomic regions that contain microsatellites, we
242 blasted two different tandem repeat motifs (TA)₁₅ and (CA)₁₅ against *AEP* transcriptomes
243 available at the HydrATLAS web portal. We found three transcripts expressed by *AEP* polyps

244 that encode repeats, the first one *c25145_g1_i04* contains TG-repeats in its first intron (**Fig 4,**
245 **Fig S2**), the second *c8134_g1_i1* encodes the Aryl-hydrocarbon receptor-Interacting Protein
246 (AIP) and contains AT-repeats in its 5' untranslated region (UTR) (**Fig 5, Fig S5**), and the third
247 one (*c21737_g1_i4*) encodes the cyclin-D-binding Myb-like Transcription Factor 1 (DMTF1)
248 and contains AT-repeats located in the 3'UTR (**Fig 6, Fig S6**).

249 Next, we validated these sequences onto genomic and transcriptomic databases publicly
250 available for *Hm-105* on National Human Genome Research Institute (NHGRI) and Compagen.
251 These three microsatellite regions were selected as they were retrieved from most databases
252 and contained a variable number of microsatellite repeats between *H. vulgaris 1 (Hm-105)*
253 and *H. carnea (AEP)*. We named these microsatellite regions *ms-c25145*, *ms-AIP* and *ms-*
254 *DMTF1* respectively; access to the corresponding transcriptomic and genomic sequences are
255 given in **Table-S3**.

256 ***The ms-c25145 polymorphism helps to discriminate between Hydra species and*** 257 ***H. vulgaris strains***

258 The TG-rich *ms-c25145* could be detected within two different *Hm-105* genomic regions
259 (*Sc4wPfr_1246*, *Sc4wPfr_396* scaffolds) and the direct PCR approach efficiently amplified the
260 *ms-c25145* genomic sequences in seven strains (*Hm-105*, *Basel1*, *Basel2*, *AEP1*, *AEP2*, *Ho_CS*,
261 *Ho_CR*), but remained inefficient in the *reg-16* strain (*H. vulgaris* group) and the *H. viridissima*
262 strain named *Nicolet*, possibly due to mismatches into primer regions (**Fig 4A, Fig S3**). The
263 patterns obtained for *ms-c25145* are quite different between *Hm-105* (four bands), *Basel1*
264 (three bands) and *Basel2* (single band), indicating that these strains can indeed be considered
265 as distinct, in agreement with the results of the *COI* phylogeny (**Fig 3**). Concerning the *AEP1*
266 and *AEP2* strains, the *ms-c25145* patterns appear quite similar, with a main band about 216
267 bp long, and a smear of larger and less intense bands (**Fig 4A**, yellow arrows). This pattern is

268 quite distinct from the sharp bands observed in *Basel2*. An intense band of similar size than in
269 *AEPs* (218 bp) is observed for *Ho_CS* and *Ho_CR* as well as some weaker and longer amplicon
270 (**Fig 4A**, orange arrows). In summary, *ms-c25145* appears as an informative marker to
271 distinguish *Hm-105*, *Basel1* and *Basel2* strains from each other, and from strains
272 representative of the *H. carnea*, *H. oligactis* and *H. viridissima* species.

273

274 **FIG 4: Analysis of the polymorphism of the TG-rich microsatellite *c25145* sequence (*ms-***
275 ***c25145*)**

276 **(A)** Amplification of the *ms-c25145* genomic sequences from seven out of nine tested strains
277 that represent three *Hydra* sub-groups, *H. vulgaris1* (*Hm-105*, *Basel1*, *Basel2* strains), *H.*
278 *carnea* (*AEP1*, *AEP2* strains) and *H. oligactis* (*Ho_CR*, *Ho_CS* strains). Yellow arrows point to a
279 smear detected in both *AEP1* and *AEP2*, orange arrows point to a faint second band detected
280 in both *Ho_CS* and *Ho_CR*. **(B)** Sequence alignment of the *ms-c25145* region. The salmon-pink
281 color box indicates the central TG-rich microsatellite region embedded within highly
282 conserved regions (grey boxes). Primer sequences used for amplification are indicated with
283 black arrows. Numbers in brackets after the strain name indicate the number of independent
284 positive sequencings, numbers at the 3' end indicate the size of the PCR product and the
285 number of TG-repeats (bold). Red writings indicate transcriptomic (t) or genomic (g)
286 sequences available on the HydrATLAS (HA) server, NHGRI *Hydra* web portal for the *Hydra* 2.0
287 genome (g2.0), or Compagen (Co) server (see **Table-S3**). **(C)** Graphical representation of the
288 different *ms-c25145* amplicons as deduced from sequencing data. Each dot corresponds to a
289 distinct amplicon confirmed by one or several sequencings as indicated by the number of
290 sequenced colonies (see **Table-S3**). Green, red and yellow color dots correspond to expected
291 sizes, lighter color dots refer to sequences with errors (PCR or sequencing), the grey dot
292 indicates missing data.

293

294 To confirm these results, we cloned the PCR products and randomly sequenced some colonies
295 from at least two animals of each strain (for sequencing details see **Table-S3**), and we found
296 the sequence size fully consistent with the observed size of the bands on the gels (**Fig 4B, 4C**).
297 Indeed, the lowest *Basel1* PCR product is slightly shorter (205 bp) than the unique *Basel2* PCR

298 product (207 bp), whereas the two other *Basel1* PCR products are 217 and 220 bp long. For
299 *Hm-105*, we retrieved sequences for three PCR products out of the four observed on the gel,
300 two corresponding to the shortest bands (192 and 203 bp) and one to the upper one (223-225
301 bp). In *AEP* samples, we retrieved multiples sequences with nucleotide polymorphism (AA
302 instead of CA repeat) that correspond to the most abundant PCR product, ranging from 212
303 to 218 pb. Finally, sequencing results confirmed that the main PCR product observed in *H.*
304 *oligactis* strains correspond to the 218 bp band, also found in *AEPs*. The sequencing data
305 provided robust results regarding the number of TG-repeats of each sequence, i.e. 6, 13 and
306 17 in *Hm-105*, 7 and 13 in *Basel1*, 8 in *Basel2*, and 14 in the *H. carnea* and *H. oligactis*
307 sequences.

308 We also analyzed the location of this *ms-cv25145* microsatellite sequence within the *ms-*
309 *cv25145* gene: It appears intronic, located after the first exon, about 245 bp downstream to
310 the 5' end (Fig S2). The *c25145* gene encodes a putative evolutionarily-conserved protein with
311 an unknown function as deduced from the alignment of the *Hydra* *c25145* deduced protein
312 product with related bilaterian sequences (Fig S4). We found similarities in the N-terminal
313 moiety (~100 first amino acids) with hypothetical proteins expressed by the sea cucumber
314 *Apostichopus japonicus* (51), the arthropods *Folsomia candida* and *Sipha flava* (aphid), the
315 mollusc *Crassostrea gigas*, the teleost fish *Myripristis murdjan*, *Sinocyclocheilus rhinoceros*
316 or *Danio rerio*. Within this domain, a signature can be identified, formed of 37 residues, from
317 which 32 are present in the *Hydra* protein (Fig S4).

318 ***The ms-AIP polymorphism helps to identify H. vulgaris and H. carnea strains***

319 The second microsatellite region (*ms-AIP*) is an AT-rich region located in the 5'UTR region of
320 the gene encoding the Aryl-hydrocarbon (AH) receptor-Interacting Protein (Fig S5). The
321 polymorphism of *ms-AIP* is more restricted than that of *ms-c25145*, as we were unable to

322 amplify these genomic sequences from the *H. oligactis* and *H. viridissima* strains (**Fig 5A**).
323 Nevertheless, *ms-AIP* is useful to discriminate between the strains within the *H. vulgaris*
324 group, i.e. *Hm-105*, *reg-16*, *Basel1*, *Basel2*, *AEP1*, *AEP2*. Two PCR products were obtained after
325 genomic amplification from *Hm-105* and *AEP2* whereas a single PCR product was amplified
326 from the other strains, with a specific size for each strain (**Fig 5A**).

327 **FIG 5: Analysis of the polymorphism of the AT-rich microsatellite region of the Aryl-**
328 **hydrocarbon receptor-Interacting Protein gene (*ms-AIP*)**

329 **(A)** Amplification of the *ms-AIP* genomic sequences in six out of nine tested strains, which
330 represent two distinct *H. vulgaris* sub-groups, *H. vulgaris 1* (*Basel1*, *Basel2*, *Hm-105*, *reg-16*)
331 and *H. carnea* (*AEP1*, *AEP2*). White arrows point to a faint band observed only in *Hm-105*
332 polyps, yellow arrows indicate a size difference between *Basel1* and *Basel2*, and the orange
333 arrows show a second band detected in *AEP2* but not in *AEP1*. **(B)** Alignment of the *ms-AIP*
334 sequences. The color boxes indicate the AT-rich central region (salmon-pink) and an A-rich
335 motif (green) embedded within highly conserved regions (grey). Primer sequences used for
336 amplification are indicated with black arrows. Numbers at the C-terminus indicate the PCR
337 product size and the number of AT-repeats (bold). Red writings indicate transcriptomic (t) or
338 genomic (g) sequences available on HydrATLAS (HA), NHGRI web portal for the *Hydra* 2.0
339 genome (g2.0) and Juliano transcriptomes (Jul), or Compagen (Co) server (see **Table-S3**). **(C)**
340 Graphical representation of the *ms-AIP* amplicons as deduced from sequencing data. Dot
341 legend as in **Fig 4**. **(D)** Amplification of *ms-AIP* in five transgenic lines *ecto-GFP* and *endo-GFP*
342 produced in uncharacterized AEP (REFs), *AEP1_Wnt3* (Vogg et al. 2019), *AEP2_203* and
343 *AEP2_293* (QS, unpublished).

344

345 The sequencing results mainly matched with the patterns detected by electrophoresis (**Fig 5B**,
346 **5C**), proving that distinct band sizes reflected stable strain-specific variations in both the
347 length of the A-rich region and the number of AT-repeats. Indeed, two distinct batches of
348 sequences were obtained for *Hm-105* (199-200 and 229-234 pb; 13 and 29-33 AT-repeats
349 respectively). The slight differences observed in the amplicon size among a given animal

350 possibly resulted from polymerase slippage during the PCR process or from an altered
351 sequencing process, as often observed in AT-rich regions (**Fig 5B**). In addition, the *ms-AIP*
352 sequences obtained from *Basel1*, *Basel2* and *reg-16* are consistent with the 198, 206 and 199
353 pb long bands observed on the gels, corresponding to 11, 13 and 11 AT-repeats respectively.
354 In contrast to *ms-c25145*, the analysis of the *ms-AIP* sequences helps distinguish between
355 *AEP1* and *AEP2*, since *AEP2* shows two bands, 204 and 212 bp long corresponding to 16 and
356 22 AT-repeats, while only the lowest band is present in *AEP1* (**Fig 5A**, orange arrow). As a
357 consequence, we consider *AEP1* and *AEP2* as two distinct strains even though their *COI* and
358 *16S* sequences are identical (**Fig 2**). Since we were able to identify different patterns in the
359 *AEP1* and *AEP2* strains, we also looked at the *ms-AIP* polymorphism in *AEP* transgenic lines
360 (**Fig 5D**). The *Q82-293* and *ecto-GFP* lines show the two-bands pattern found in *AEP2* while
361 the *Wnt3::GFP*, *endo-GFP* and *Q82-203* lines show the same single-band pattern than *AEP1*.
362 In summary, the analysis of the *ms-AIP* patterns are informative to identify and characterize
363 strains of the *H. vulgaris 1* species. In addition, in contrast to *ms-c25145*, *ms-AIP* provides a
364 useful marker for the *AEP* strains and *AEP* transgenic lines.

365 ***The ms-DMTF1 microsatellite helps to discriminate between the H. carnea AEP*** 366 ***lines***

367 The third microsatellite sequence (*ms-DMTF1*) is also AT-rich but located in the 3' UTR of the
368 *cyclin-D-binding Myb-Like transcription factor 1* gene (**Fig S6**). The *ms-DMTF1* primers were
369 designed for *H. carnea* strains and are thus only suitable for strains that belong to the *H.*
370 *vulgaris* group (**Fig 6A**). Accordingly, they are useful to discriminate between animals of this
371 *H. vulgaris* group. The analysis of the *ms-DMTF1* polymorphism does not show variability
372 between *AEP1* and *AEP2* but remains useful to distinguish the *endo-GFP* transgenic animals
373 from all other *AEPs* (**Fig 6**). In fact, all the *AEP* strains and lines we tested here but the

374 transgenic line *endo-GFP*, provide a two-band pattern, the lowest band being similar in size
375 with the single one found in the *endo-GFP* (Fig 6B). By shot-gun sequencing of the PCRs
376 products from different *AEP* animals, we found that the sequence of the upper band is 118 bp
377 long (Fig 6C, 6D). In complement, the sequencing data obtained in the *endo-GFP* animals
378 identified a PCR product that corresponds to 104 bp. Interestingly, available transcriptomes
379 confirm the existence of both sequences (Fig 6C and Table-S3).

380

381 **FIG 6: Analysis of the polymorphism of the AT-rich microsatellite detected in the Cyclin-D-**
382 **Binding Myb-Like Transcription Factor 1 gene (*ms-DMTF1*)**

383 **(A, B)** Amplification of the *ms-DMTF1* genomic sequence is restricted to the *AEP* strains, either
384 unmodified (*AEP1*, *AEP2*) or transgenic (*Q82-293*, *ecto-GFP*, *Wnt3::GFP*, *endo-GFP*) lines. **(C)**
385 Alignment of the *ms-DMTF1* sequences. The color boxes indicate the AT-rich central region
386 (salmon-pink) embedded within highly conserved regions (grey). Primer sequences used for
387 amplification are indicated with black arrows. Numbers in brackets after the strain name
388 indicate the number of independent positive sequencings, numbers at the 3' end indicate the
389 size of the PCR product and the number of AT-repeats (bold). Red writings indicate
390 transcriptomic (t) or genomic (g) sequences available on HydrATLAS (HA) server, NHGRI web
391 portal for the *Hydra* 2.0 genome (g2.0) and Juliano transcriptomes (Jul), or Compagen (Co)
392 server (see Table-S3). **(D)** Graphical representation of the size of the *ms-DMTF1* amplicons as
393 deduced from sequencing data. Red color dots correspond to expected sizes, the grey dot
394 indicates missing data.

395 **Comparative analysis of the information brought by microsatellite barcoding**

396 To establish the respective barcode values of the *ms-c25145*, *ms-AIP* and *ms-DMTF1*
397 microsatellites (Fig 7), we compared the results obtained in the 36 strain/species pairs tested
398 for each microsatellite. From the analysis of these three microsatellites we deduced four levels
399 of information, (1) informative when the patterns are distinct between the two
400 strains/species, (2) partially informative when microsatellite amplification is observed in one
401 strain/species but not in the other, (3) or when the patterns obtained are identical between

402 the two strains/species, (4) non-informative when amplification is not observed in either
403 strain/species.

404 Among these three microsatellites, *ms-c25145* is the most informative as the only one
405 amplified in three distinct species (*H. vulgaris 1*, *H. carnea*, *H. oligactis*), providing a positive
406 discrimination in 29 pairs (80.6%), either based on specific patterns as observed in 15 pairs
407 (41.7%) or on an amplification restricted to a single strain/species in 14 pairs (38.9%). The *ms-*
408 *AIP* is amplified in *H. vulgaris 1* and *H. carnea*, providing a positive discrimination in 30 pairs,
409 based on specific patterns in only 12 pairs (40%) and on an amplification restricted to a single
410 strain/species in 18 pairs (60%). Finally, *ms-DMTF1* is only amplified in the *AEP1* and *AEP2*
411 strains, providing a similar pattern in eight pairs, but a distinct one in some transgenic strains.
412 We concluded that the approach presented here fulfilled our initial objective since it allowed
413 us to properly characterize all strains of the *H. vulgaris* group used in our laboratory, i.e. strains
414 *Hm-105*, *Basel1*, *Basel2* and *reg-16* of the species *H. vulgaris-1* as well as strains *AEP1*, *APE2*
415 of the species *H. carnea*. By contrast, the phylogenetic approaches based on *COI* and *16S*
416 sequences had failed as the *COI* and *16S* sequences were identical between some strains.

417 **Fig 7: Summary scheme showing the value of each microsatellite for efficient discrimination**
418 **between *Hydra* species and *Hydra* strains**

419 ***Analysis of speciation events in *H. vulgaris* based on the microsatellite***
420 ***signatures***

421 Although the region surrounding the microsatellites sequences is quite conserved between all
422 strains, we observed systematic differences between *H. vulgaris 1* and *H. carnea* strains in the
423 organization of the amplified regions such as the TAGTCAAAGTAGTACA deletion in the
424 upstream non-conserved region of *ms-c25145* in *H. vulgaris 1* strains (Fig 4B), or the size
425 difference in the A-rich region in *ms-AIP* (Fig 5B). The conserved deletions in one of the two
426 subgroups and the differences in the microsatellite motifs suggest that the genetic flux

427 between *H. carnea* strains (*AEP*) and *H. vulgaris 1* strains (*Hm-101*, *Basel1*, *Basel2*, *reg-16*) no
428 longer exists, suggesting that *H. vulgaris 1* and *H. carnea* can be considered as two cryptic
429 species (52). This hypothesis requires further confirmation that could be obtained by
430 amplifying the *ms-c25145*, *ms-AIP* and additional microsatellite sequences from
431 representative animals of the 14 hypothetical species reported by Schwentner and Bosch (14).

432 **DISCUSSION**

433 ***The direct dissociation of soft tissues provides quality templates for genomic*** 434 ***PCR amplification***

435 Genomic extractions for multiple samples as well as for population genetics studies can be
436 rapid but costly when commercial kits are used, or time-consuming and risky when reagents
437 that are rather toxic to humans and/or the environment are used (e.g. guanidium thiocyanate,
438 β -mercaptoethanol). For these reasons, we have tried here to bypass the genomic extraction
439 step and to use directly as PCR substrate dissociated *Hydra* tissues that we call "macerate
440 extracts". The rapid and inexpensive protocol we present here is based on the mechanical
441 dissociation of the tissues, which reliably allows the PCR amplification of mitochondrial and
442 nuclear DNA. This procedure is now commonly used in our laboratory, not only to amplify
443 microsatellite sequences and detect in *Hydra* cultures suspected contamination by polyps of
444 other strains, but also to amplify genomic sequences of genes of interest for directly
445 sequencing or insertion into plasmid vectors. We also successfully applied this procedure to
446 fixed *Hydra* tissues as reported above, as well as poriferan larvae (e.g. *Oscarella lobularis*, not
447 shown). Therefore, this protocol can be effectively applied to soft tissues from any developing
448 or adult organisms, especially when small amounts of tissue are available.

449 ***Systematize characterization of Hydra strains to improve data reproducibility***

450 The microsatellite barcoding approach reported here offers a series of important advantages
451 in that it is (i) *sensitive*, detecting a 2 bp shift in amplicon size, (ii) *simple*, requiring no
452 chemicals or materials other than those used in ordinary PCR as in conventional barcoding
453 approaches, (iii) *fast*, with data being acquired in less than a day, (iv) *robust* as it provides
454 reproducible results. The immediate use of macerate extracts could be a possible limitation
455 of this procedure. Indeed, we did not test the quality of these macerate extracts after their
456 storage in a frozen state, assuming that nucleic acid degradation would occur. Nevertheless,
457 we were able to amplify genomic DNA obtained after mechanical dissociation from intact
458 frozen animal samples, implying that fresh material is not an absolute requirement.

459 In the context of life sciences where reproducibility can be a challenge (53,54), the
460 development of tools to properly characterize the animals we work with appears to be a
461 cornerstone towards more effective research. Indeed, *Hydra* laboratories use a wide variety
462 of strains that are known to respond differently to chemical treatments or show variable
463 sensitivity to gene expression silencing by RNAi. This procedure opens up the possibility of
464 conducting blind clonal culture experiments, where the sensitivity of different strains to toxic
465 substances, environmental stresses such as temperature changes can be compared. Indeed,
466 as the microsatellite barcode procedure can be easily replicated on batches of unique polyps,
467 it represents a major asset for discriminating among phenotypically similar polyps those that
468 are genetically different, and vice versa.

469 ***Possible mechanisms explaining the strain-specific variations observed in***
470 ***Hydra microsatellite sequences***

471 Karyotyping on *Hm-105* revealed that *Hydra* are diploid animals ($2n=30$) (55). It is therefore
472 not surprising to observe either a single band or more frequently the same band completed

473 by a second band, reflecting the homozygous versus heterozygous status of a given animal
474 respectively. On the other hand, we interpret the differences in band size observed in animals
475 of different strains as different alleles. Nevertheless, we have clearly observed and sequenced
476 more than two different bands in the same polyp (see *ms-c25145* in *Hm-105* and *Basel1*). As
477 mentioned above, the *ms-c25145* primers we have designed can amplify two different regions
478 of the *Hm-105* genome (*Sc4wPen_1246*, *Sc4wPen_396*), which explains why four bands can
479 be observed in this strain (twice two alleles). The most parsimonious scenario would be that
480 these two regions result from a recent single gene duplication that occurred in the common
481 ancestor of the *Hm-105* and *Basel1* strains, without affecting the other strains tested here
482 where only one copy is detected.

483 The microsatellite barcoding might also reveal some genetic mosaicism, as suspected from
484 the four-band and three-band patterns observed for *ms-c25145*. Genetic mosaicism is defined
485 as genetic variations acquired post-zygotically in cells of an individual developed from a single
486 zygote, a phenomena frequently observed in plants and clonal animals as well as in humans
487 (56,57). In clonal animals as cnidarians, the segregation of germ cells does not occur during
488 early embryonic development and mutations affecting somatic cells as well as germ cells can
489 accumulate over the multiple divisions of multipotent stem cells. In *Hydra*, beside the
490 interstitial stem cell population that can transiently provide germ cells, the two epithelial stem
491 cell populations also continuously cycle over the lifetime of the animal, potentially
492 accumulating somatic mutations independently. This mechanism provides the opportunity for
493 additional genetic variations within the same animal as observed in leaf cells (58).

494 ***The microsatellite analysis supports the hypothesis of cryptic species within the***
495 ***H. vulgaris group***

496 With the development of "omics" over the last decade, the subdivision of the genus *Hydra*
497 into four main species, as initially proposed on morphological, developmental and cellular
498 criteria, appears more complicated. Indeed, if molecular phylogenetic analyses have
499 confirmed this four group classification, they have also highlighted the existence of several
500 subgroups within each species (13–16), and one issue concerns the specification of separate
501 species within the *H. vulgaris* group. For instance, Martinez et coll. (13) consider the *H.*
502 *vulgaris* group as a single species clustering into five main sub-groups defined by their
503 geographical distribution: South Africa, North America (e.g. *AEP*), South America, Eurasia (e.g.
504 *Basel*, *Zürich*, *Hm-105*) and Oceania. Similarly, Kawaida et coll. (12) consider the *H. vulgaris*
505 group as forming a single species but described three main sub-groups called *H. vulgaris*, *H.*
506 *carnea* and *H. sp.*

507 In contrast, Schwentner and Bosch (14) suggest that the *H. vulgaris* group is more complex
508 than expected, revealing at least 14 distinct subgroups, each representing a hypothetical
509 species. They propose to cluster within a single *H. carnea* species the *H. carnea*, *H. littoralis*
510 and the majority of the North American *H. vulgaris* strains, including the *AEP* strains. As a
511 consequence, the *H. vulgaris* strains from Europe and Japan, named by these authors *H.*
512 *vulgaris 1* would form a distinct *H. vulgaris* species, corresponding to that initially described
513 in the 18e century by Trembley (1). The analysis of the microsatellite polymorphism reported
514 in the present study supports this view as the data obtained on six wild-type strains that
515 belong to the *H. vulgaris* group point to a divergence between the North American (*AEP*) and
516 the Eurasian (*Hm-105*, *reg-16*, *Basel1*, *Basel2*) sequences. The acquisition of a genome for
517 each sub-group would help to perform meta-analyses and analysis of single-nucleotide

518 polymorphism to state on *H. vulgaris* species delimitation as recently done for the
519 *Ophioderma* sea stars (59).

520 CONCLUSION

521 With this study, we implemented a powerful barcoding approach based on microsatellite
522 polymorphism for strains belonging to the *H. vulgaris* group. The use of this approach should
523 enhance the reproducibility of experiments conducted in different laboratories by allowing
524 the correct identification of each strain, including the AEP transgenic lines, in order to conduct
525 unbiased experiments on well-characterized polytypes. Data obtained on six wild-type strains
526 belonging to the main hydra species used in experimental biology, namely *H. vulgaris* (referred
527 to here as *H. vulgaris1*) and *H. carnea*, tend to confirm that the *H. vulgaris* group actually
528 covers a set of cryptic species rather than a single species. We believe that microsatellite
529 polymorphism analysis can help discover speciation events, thus representing a
530 complementary approach to phylogenetic analyses aimed at identifying *Hydra* species.

531 Acknowledgements

532 This work was supported by the Swiss National Science Foundation (SNF grants
533 31003_169930), the Claraz donation and the Canton of Geneva.

534 Contributions

535 QS proposed the initial concept and design of the project; QS identified the microsatellites
536 and designed the primers. DPC and QS implemented the PCR approach and performed the
537 PCRs. CP and QS prepared the samples for sequencing. BG supervised the research. BG and
538 QS discussed the results and wrote the manuscript.

539

540 REFERENCES

- 541 1. Trembley A. Mémoires pour servir à l'histoire d'un genre de polypes d'eau douce, à bras en forme
542 de cornes. Leiden; 1744.
- 543 2. Watanabe H, Hoang VT, Mattner R, Holstein TW. Immortality and the base of multicellular life:
544 Lessons from cnidarian stem cells. *Semin Cell Dev Biol.* 2009; 20: 1114–25.
- 545 3. Galliot B, Quiquand M. A two-step process in the emergence of neurogenesis. *Eur J Neurosci.*
546 2011; 34: 847–862.
- 547 4. Galliot B. Hydra, a fruitful model system for 270 years. *Int J Dev Biol.* 2012; 56: 411–423.
- 548 5. Augustin R, Fraune S, Franzenburg S, Bosch TC. Where simplicity meets complexity: hydra, a
549 model for host-microbe interactions. *Adv Exp Med Biol.* 2012; 710: 71–81.
- 550 6. Rachamim T, Sher D. What Hydra can teach us about chemical ecology how a simple, soft
551 organism survives in a hostile aqueous environment. *Int J Dev Biol.* 2012; 56: 605–611.
- 552 7. Murugadas A, Zeeshan M, Thamaraiselvi K, Ghaskadbi S, Akbarsha MA. Hydra as a model
553 organism to decipher the toxic effects of copper oxide nanorod: Eco-toxicogenomics approach.
554 *Sci Rep.* 2016; 15: 29663.
- 555 8. Schenkelaars Q, Boukerch S, Galliot B. Freshwater Cnidarian Hydra: A Long-lived Model for Aging
556 Studies. In: Rattan SIS, editor. *Encyclopedia of Biomedical Gerontology*, Academic Press; 2020.
557 p. 115–127.
- 558 9. Sugiyama T, Fugisawa T. Genetic analysis of developmental mechanisms in hydra. I. Sexual
559 reproduction of Hydra magnipapillata and isolation of mutants. *Growth Dev Differ.* 1977; 19:
560 187–200.
- 561 10. Sugiyama T, Fujisawa T. Genetic analysis of developmental mechanisms in Hydra. VII. Statistical
562 analyses of developmental morphological characters and cellular compositions. *Dev Growth*
563 *Differ.* 1979; 21: 361–375.
- 564 11. Campbell RD. A new species of Hydra (Cnidaria: Hydrozoa) from North America with comments
565 on species clusters within the genus. *Zool J Linn Soc.* 1987; 91: 253–263.
- 566 12. Holstein T, Emschermann P. Zytologie. In: Schwoerbel J, Zwick P, editors. *Cnidaria: Hydrozoa,*
567 *Kamptozoa.* Stuttgart: Gustav Fisher Verlag; 1995. p. 5–15. (Süßwasserfauna von Mitteleuropa;
568 vol. 1).
- 569 13. Hemmrich G, Anokhin B, Zacharias H, Bosch TC. Molecular phylogenetics in Hydra, a classical
570 model in evolutionary developmental biology. *Mol Phylogenet Evol.* 2007; 44: 281–290.
- 571 14. Kawaida H, Shimizu H, Fujisawa T, Tachida H, Kobayakawa Y. Molecular phylogenetic study in
572 genus Hydra. *Gene.* 2010; 468: 30–40.
- 573 15. Martinez DE, Iniguez AR, Percell KM, Willner JB, Signorovitch J, Campbell RD. Phylogeny and
574 biogeography of Hydra (Cnidaria: Hydridae) using mitochondrial and nuclear DNA sequences.
575 *Mol Phylogenet Evol.* 2010; 57: 403–410.
- 576 16. Schwentner M, Bosch TC. Revisiting the age, evolutionary history and species level diversity of
577 the genus Hydra (Cnidaria: Hydrozoa). *Mol Phylogenet Evol.* 2015; 91: 41–55.

- 578 17. Ito T. A new fresh-water polyp, *Hydra magnipapillata*, n. sp. from Japan. In: ***Science Reports of***
579 ***the Tohoku University***. 1947. p. 6–10.
- 580 18. Martin VJ, Littlefield CL, Archer WE, Bode HR. Embryogenesis in hydra. ***Biol Bull***. 1997; 192: 345–
581 363.
- 582 19. Wittlieb J, Khalturin K, Lohmann JU, Anton-Erxleben F, Bosch TCG. Transgenic Hydra allow in vivo
583 tracking of individual stem cells during morphogenesis. ***Proc Natl Acad Sci U S A***. 2006; 103:
584 6208–6211.
- 585 20. Schaller HC, Schmidt T, Flick K, Grimmelikhuijzen CPJ. Analysis of morphogenetic mutants of
586 hydra. I. The aberrant. ***Roux Arch Dev Biol***. 1977; 193–206.
- 587 21. Schaller HC, Schmidt T, Flick K, Grimmelikhuijzen CPJ. Analysis of morphogenetic mutants of
588 hydra. II. The non-budding mutant. ***Roux Arch Dev Biol***. 1977; 183: 207–214.
- 589 22. Schaller HC, Schmidt T, Flick K, Grimmelikhuijzen CPJ. Analysis of morphogenetic mutants of
590 hydra. III. Maxi and Mini. ***Roux Arch Dev Biol***. 1977; 183: 215–222.
- 591 23. Takano J, Sugiyama T. Genetic analysis of developmental mechanisms in hydra. XVI. Effect of food
592 on budding and developmental gradients in a mutant strain L4. ***J Embryol Exp Morphol***. 1985;
593 90: 123–138.
- 594 24. Sugiyama T, Fujisawa T. Genetic analysis of developmental mechanisms in Hydra. III.
595 Characterization of a regeneration deficient strain. ***J Embryol Exp Morph***. 1977; 42: 65–77.
- 596 25. Sugiyama T. Roles of head-activation and head-inhibition potentials in pattern formation of
597 Hydra: Analysis of a multi-headed mutant strain. ***Am Zool***. 1982; 22: 27–34.
- 598 26. Zeretzke S, Berking S. Analysis of a Hydra mutant which produces extra heads along its body axis.
599 ***Int J Dev Biol***. 1996; Suppl 1:271S.
- 600 27. Sugiyama T, Fujisawa T. Genetic analysis of developmental mechanisms in Hydra. II. Isolation and
601 characterization of an interstitial cell-deficient strain. ***J Cell Sci***. 1978; 29: 35–52.
- 602 28. Marcum BA, Fujisawa T, Sugiyama T. A mutant hydra strain (sf-1) containing temperature-
603 sensitive interstitial cells. In: Tardent P, Tardent R, editors. ***Developmental and Cellular Biology***
604 ***of Coelenterates***. Amsterdam: Elsevier/North Holland; 1980. p. 429–434.
- 605 29. Chera S, Ghila L, Wenger Y, Galliot B. Injury-induced activation of the MAPK/CREB pathway
606 triggers apoptosis-induced compensatory proliferation in hydra head regeneration. ***Dev Growth***
607 ***Differ***. 2011; 53: 186–201.
- 608 30. Glauber KM, Dana CE, Park SS, Colby DA, Noro Y, Fujisawa T, et al. A small molecule screen
609 identifies a novel compound that induces a homeotic transformation in Hydra. ***Development***.
610 2013; 140: 4788–4796.
- 611 31. Schenkelaars Q, Tomczyk S, Wenger Y, Ekundayo K, Girard V, Buzgariu W, et al. Hydra, a model
612 system for deciphering the mechanisms of aging and resistance to aging. In: Conn PM, Ram JL,
613 editors. ***Conn's Handbook For Models On Human Aging***. 2nd ed. Elsevier; 2018.
- 614 32. Tomczyk S, Suknovic N, Schenkelaars Q, Wenger Y, Ekundayo K, Buzgariu W, et al. Deficient
615 autophagy in epithelial stem cells drives aging in the freshwater cnidarian *Hydra*. ***Development***.
616 2020; 147: dev177840.

- 617 33. David CN, Fujisawa T, Bosch TCG. Interstitial stem cell proliferation in hydra: Evidence for strain-
618 specific regulatory signals. *Dev Biol.* 1991; 148: 501–507.
- 619 34. Chapman JA, Kirkness EF, Simakov O, Hampson SE, Mitros T, Weinmaier T, et al. The dynamic
620 genome of Hydra. *Nature.* 2010; 464: 592–596.
- 621 35. Wenger Y, Galliot B. RNAseq versus genome-predicted transcriptomes: a large population of
622 novel transcripts identified in an Illumina-454 Hydra transcriptome. *BMC Genomics.* 2013; 14:
623 204.
- 624 36. Wenger Y, Galliot B. Punctuated emergences of genetic and phenotypic innovations in
625 eumetazoan, bilaterian, euteleostome, and hominidae ancestors. *Genome Biol Evol.* 2013; 5:
626 1949–1968.
- 627 37. Petersen HO, Hoger SK, Looso M, Lengfeld T, Kuhn A, Warnken U, et al. A Comprehensive
628 Transcriptomic and Proteomic Analysis of Hydra Head Regeneration. *Mol Biol Evol.* 2015; 32:
629 1928–1947.
- 630 38. Juliano CE, Reich A, Liu N, Götzfried J, Zhong M, Uman S, et al. PIWI proteins and PIWI-interacting
631 RNAs function in Hydra somatic stem cells. *Proc Natl Acad Sci U S A.* 2014 Jan 7;111(1):337–42.
- 632 39. Wenger Y, Buzgariu W, Reiter S, Galliot B. Injury-induced immune responses in Hydra. *Semin*
633 *Immunol.* 2014; 26: 277–294.
- 634 40. Wenger Y, Buzgariu W, Galliot B. Loss of neurogenesis in Hydra leads to compensatory regulation
635 of neurogenic and neurotransmission genes in epithelial cells. *Philos Trans R Soc Lond B Biol Sci.*
636 2016; 371: 20150040.
- 637 41. Wenger Y, Buzgariu W, Perruchoud C, Loichot G, Galliot B. Generic and context-dependent gene
638 modulations during *Hydra* whole body regeneration. *bioRxiv.* 2019; 587147.
- 639 42. Siebert S, Farrell JA, Cazet JF, Abeykoon Y, Primack AS, Schnitzler CE, et al. Stem cell
640 differentiation trajectories in *Hydra* resolved at single-cell resolution. *Science.* 2019; 365:
641 eaav9314.
- 642 43. Hemmrich G, Khalturin K, Boehm AM, Puchert M, Anton-Erxleben F, Wittlieb J, et al. Molecular
643 signatures of the three stem cell lineages in hydra and the emergence of stem cell function at
644 the base of multicellularity. *Mol Biol Evol.* 2012; 29: 3267–3280.
- 645 44. Vieira MLC, Santini L, Diniz AL, Munhoz C de F. Microsatellite markers: what they mean and why
646 they are so useful. *Genet Mol Biol.* 2016; 39: 312–328.
- 647 45. Pena SDJ, Chakraborty R. Paternity testing in the DNA era. *Trends Genet.* 1994; 10: 204–209.
- 648 46. Manjunath BC, Chandrashekar BR, Mahesh M, Vatchala Rani RM. DNA Profiling and forensic
649 dentistry – A review of the recent concepts and trends. *J Forensic Leg Med.* 2011; 18: 191–197.
- 650 47. Anton-Erxleben F, Thomas A, Wittlieb J, Fraune S, Bosch TC. Plasticity of epithelial cell shape in
651 response to upstream signals: a whole-organism study using transgenic Hydra. *Zool.* 2009; 112:
652 185–94.
- 653 48. Nakamura Y, Tsiairis CD, Ozbek S, Holstein TW. Autoregulatory and repressive inputs localize
654 Hydra Wnt3 to the head organizer. *Proc Natl Acad Sci U S A.* 2011; 108: 9137–9142.

- 655 49. Vogg MC, Beccari L, Ollé LI, Rampon C, Vríz S, Perruchoud C, et al. An evolutionarily-conserved
656 Wnt3/ β -catenin/Sp5 feedback loop restricts head organizer activity in *Hydra*. **Nat Commun.**
657 2019; 10: 312.
- 658 50. Guindon S, Dufayard JF, Lefort V, Anisimova M, Hordijk W, Gascuel O. New algorithms and
659 methods to estimate maximum-likelihood phylogenies: assessing the performance of PhyML 3.0.
660 **Syst Biol.** 2010; 59: 307–321.
- 661 51. Zhang X, Sun L, Yuan J, Sun Y, Gao Y, Zhang L, et al. The sea cucumber genome provides insights
662 into morphological evolution and visceral regeneration. Tyler-Smith C, editor. **PLOS Biol.** 2017;
663 15: e2003790.
- 664 52. Bickford D, Lohman DJ, Sodhi NS, Ng PKL, Meier R, Winker K, et al. Cryptic species as a window
665 on diversity and conservation. **Trends Ecol Evol.** 2007; 22: 148–155.
- 666 53. Baker M. A Nature survey lifts the lid on how researchers view the ‘crisis’ rocking science and
667 what they think will help. **Nature.** 2015: 3.
- 668 54. Fanelli D. Opinion: Is science really facing a reproducibility crisis, and do we need it to? **Proc Natl**
669 **Acad Sci U S A.** 2018; 115: 2628–2631.
- 670 55. Anokhin BA, Kuznetsova VG. FISH-based karyotyping of *Pelmatohydraoligactis* (Pallas, 1766),
671 *Hydraoxycnida* Schulze, 1914, and *H.magnipapillata* Ito, 1947 (Cnidaria, Hydrozoa). **Comp**
672 **Cytogenet.** 2018; 12: 539–548.
- 673 56. Gill DE, Chao L, Perkins SL, WolJ JB. Genetic Mosaicism in Plants and Clonal Animals. **Annu Rev**
674 **Ecol Evol Syst.** 1995; 26: 423-444.
- 675 57. Campbell IM, Shaw CA, Stankiewicz P, Lupski JR. Somatic mosaicism: implications for disease and
676 transmission genetics. **Trends Genet.** 2015; 31: 382–392.
- 677 58. Diwan D, Komazaki S, Suzuki M, Nemoto N, Aita T, Satake A, et al. Systematic genome sequence
678 differences among leaf cells within individual trees. **BMC Genomics.** 2014; 15: 142.
- 679 59. Weber AA-T, Stöhr S, Chenuil A. Species delimitation in the presence of strong incomplete lineage
680 sorting and hybridization: Lessons from *Ophioderma* (Ophiuroidea: Echinodermata). **Mol**
681 **Phylogenet Evol.** 2019; 131: 138–148.
- 682

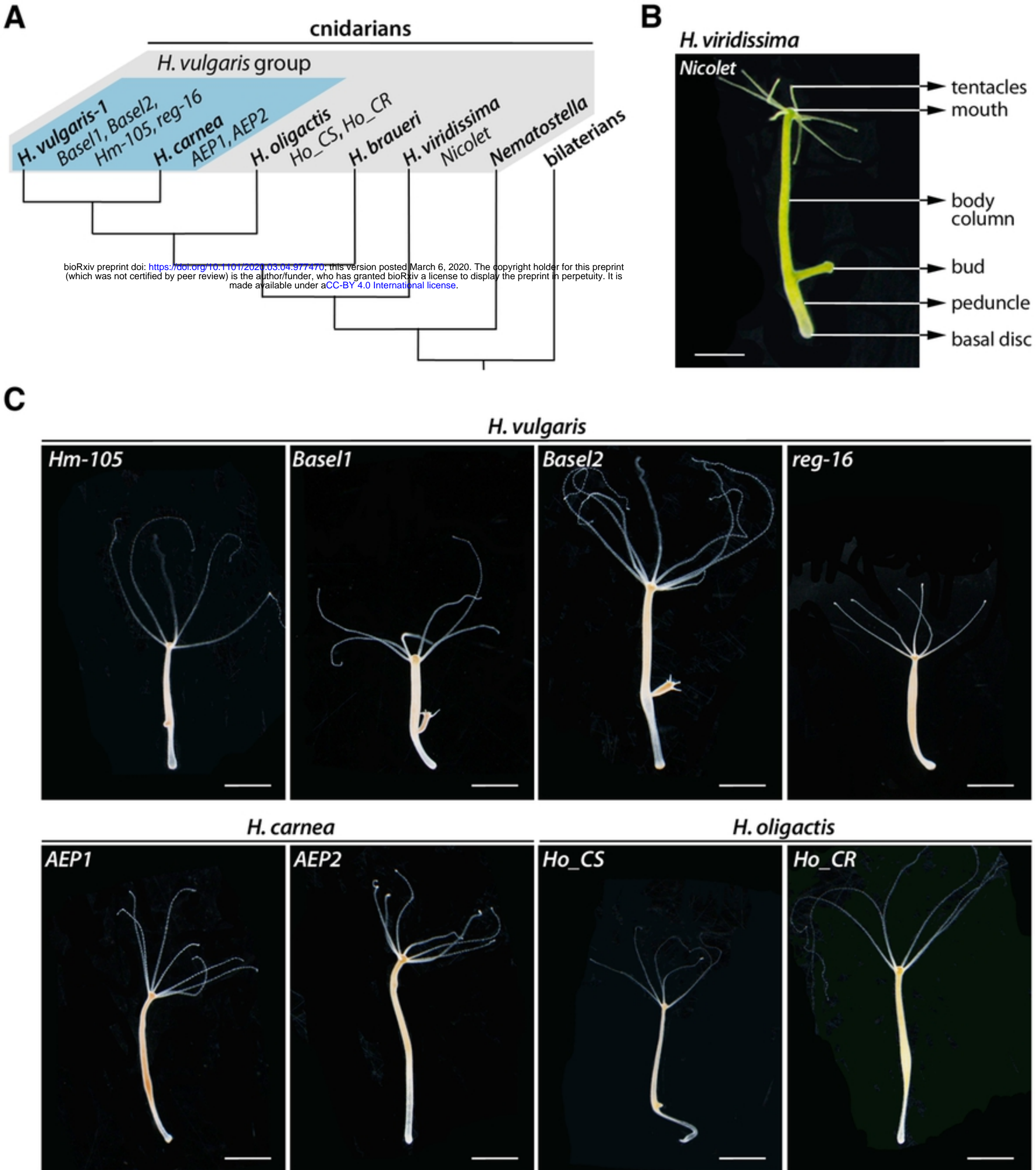
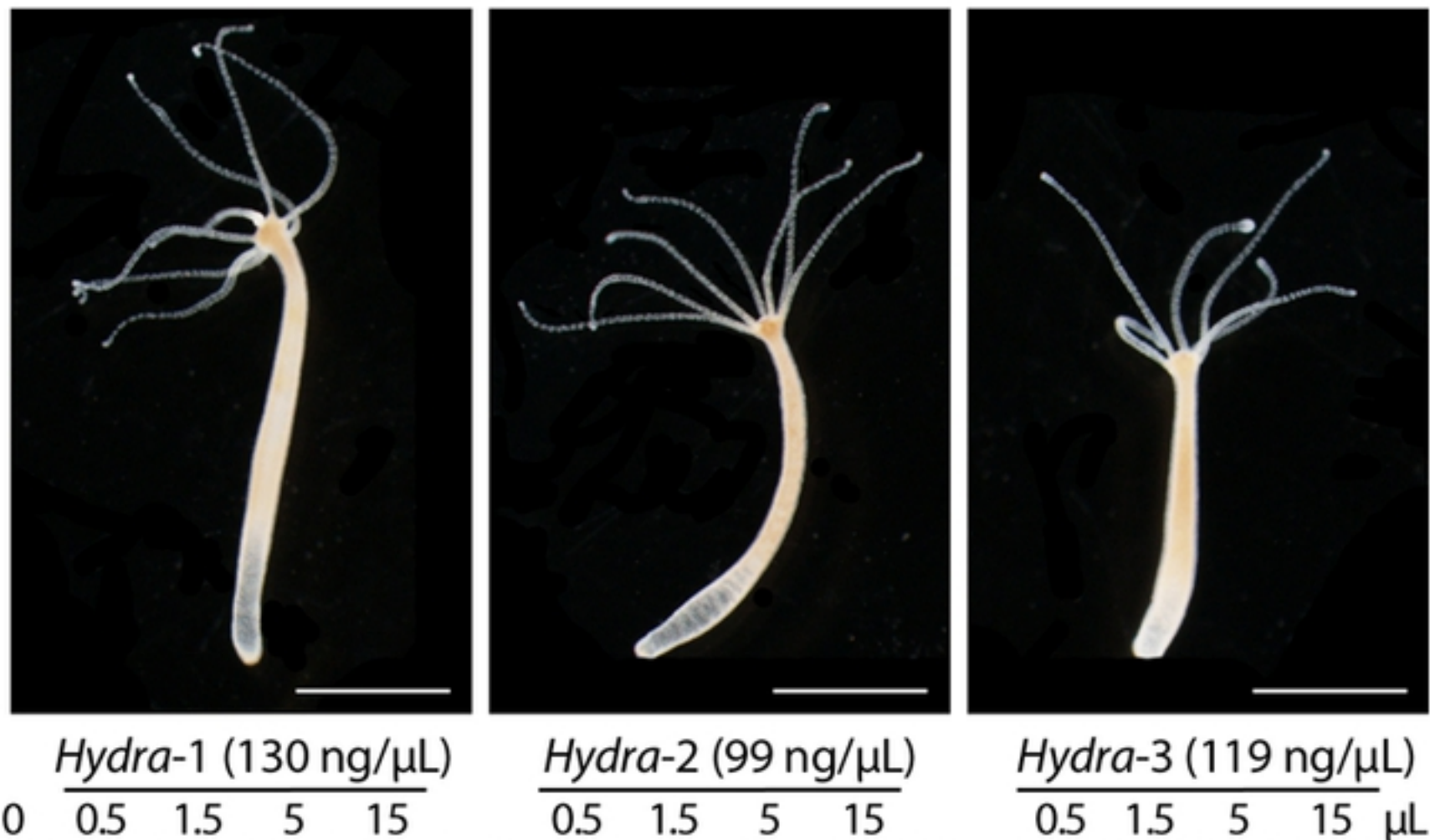


Figure 1

A

bioRxiv preprint doi: <https://doi.org/10.1101/2020.03.04.977470>; this version posted March 6, 2020. The copyright holder for this preprint (which was not certified by peer review) is the author/funder, who has granted bioRxiv a license to display the preprint in perpetuity. It is made available under aCC-BY 4.0 International license.

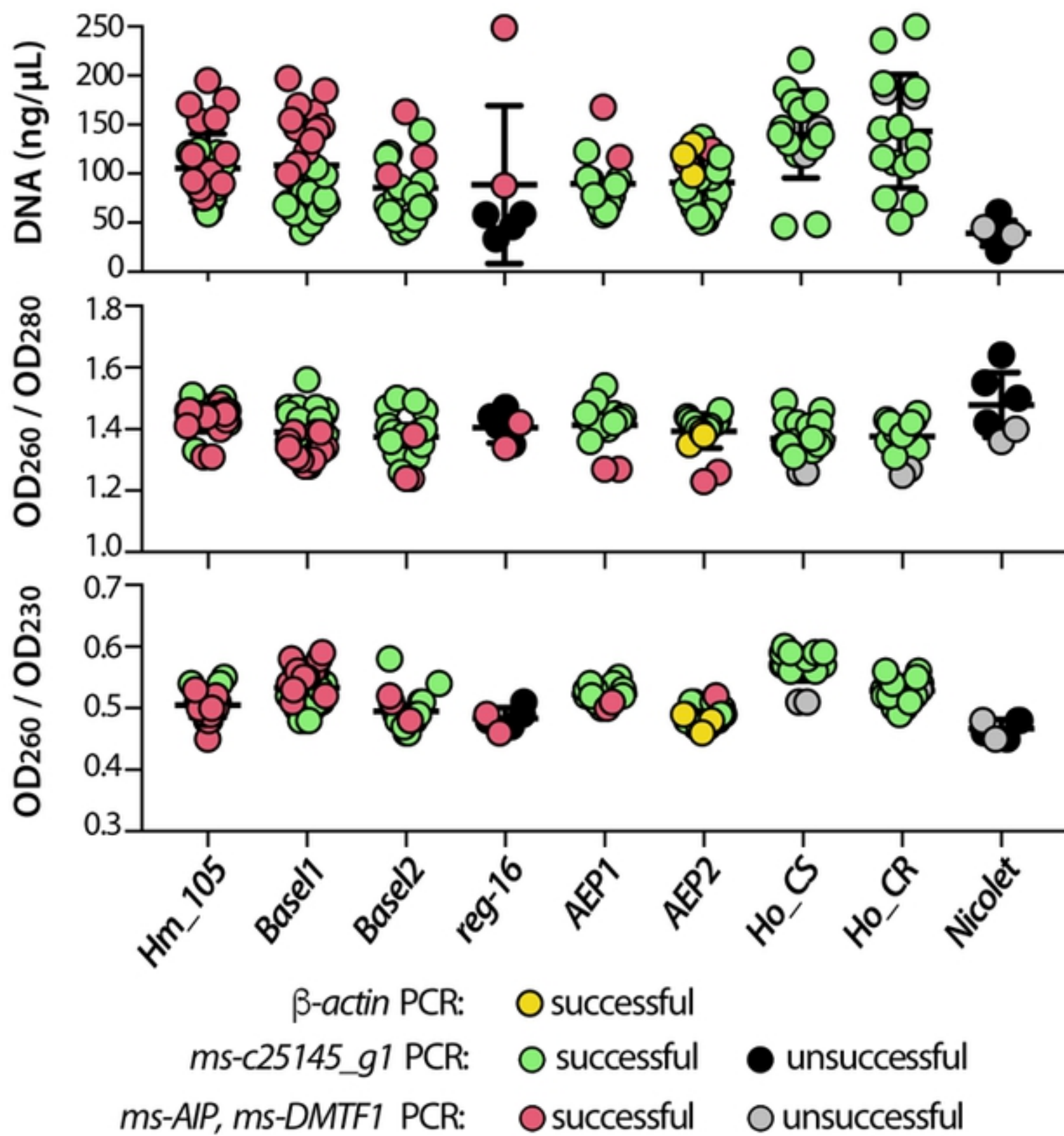
B

Figure 2

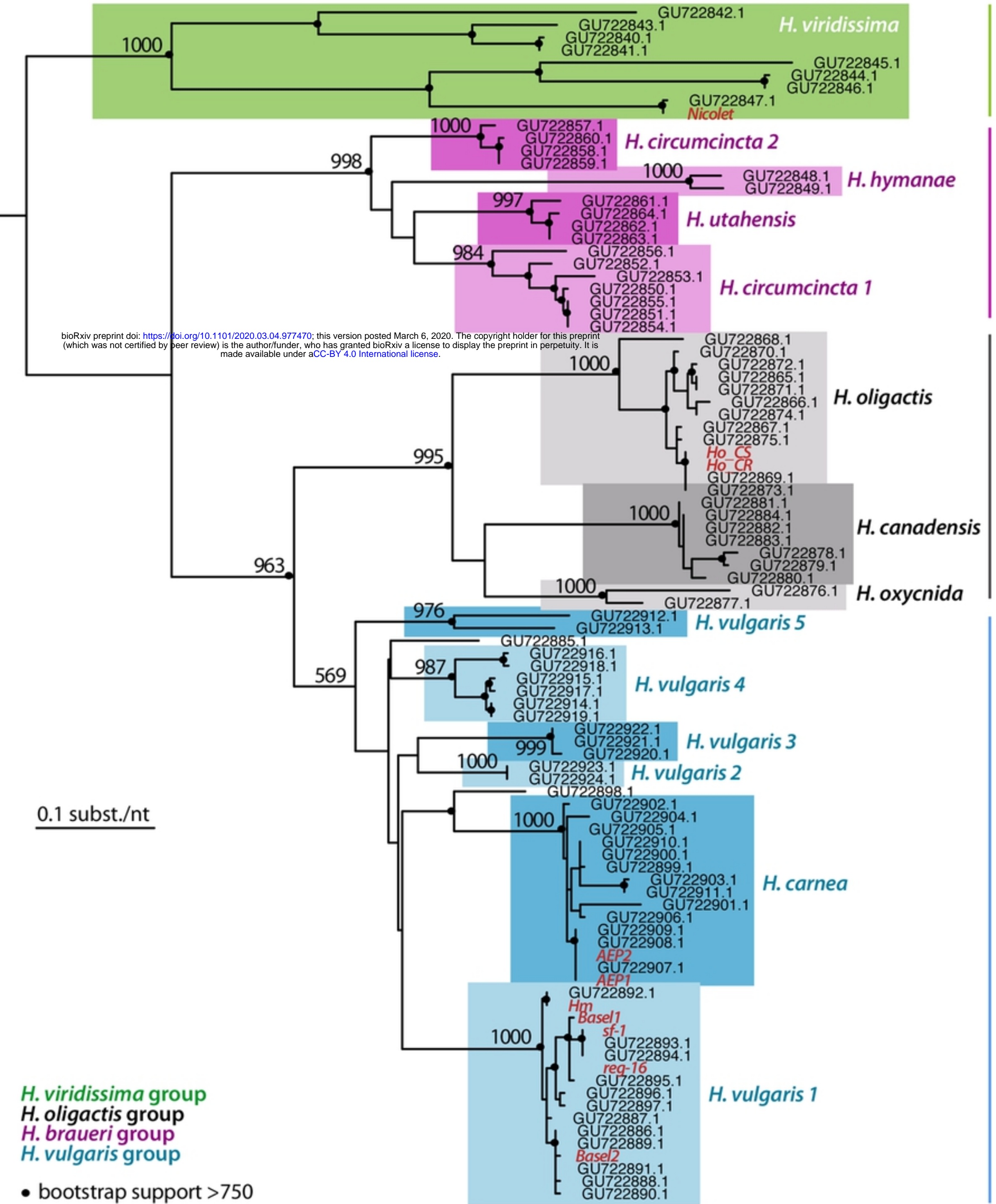


Figure 3

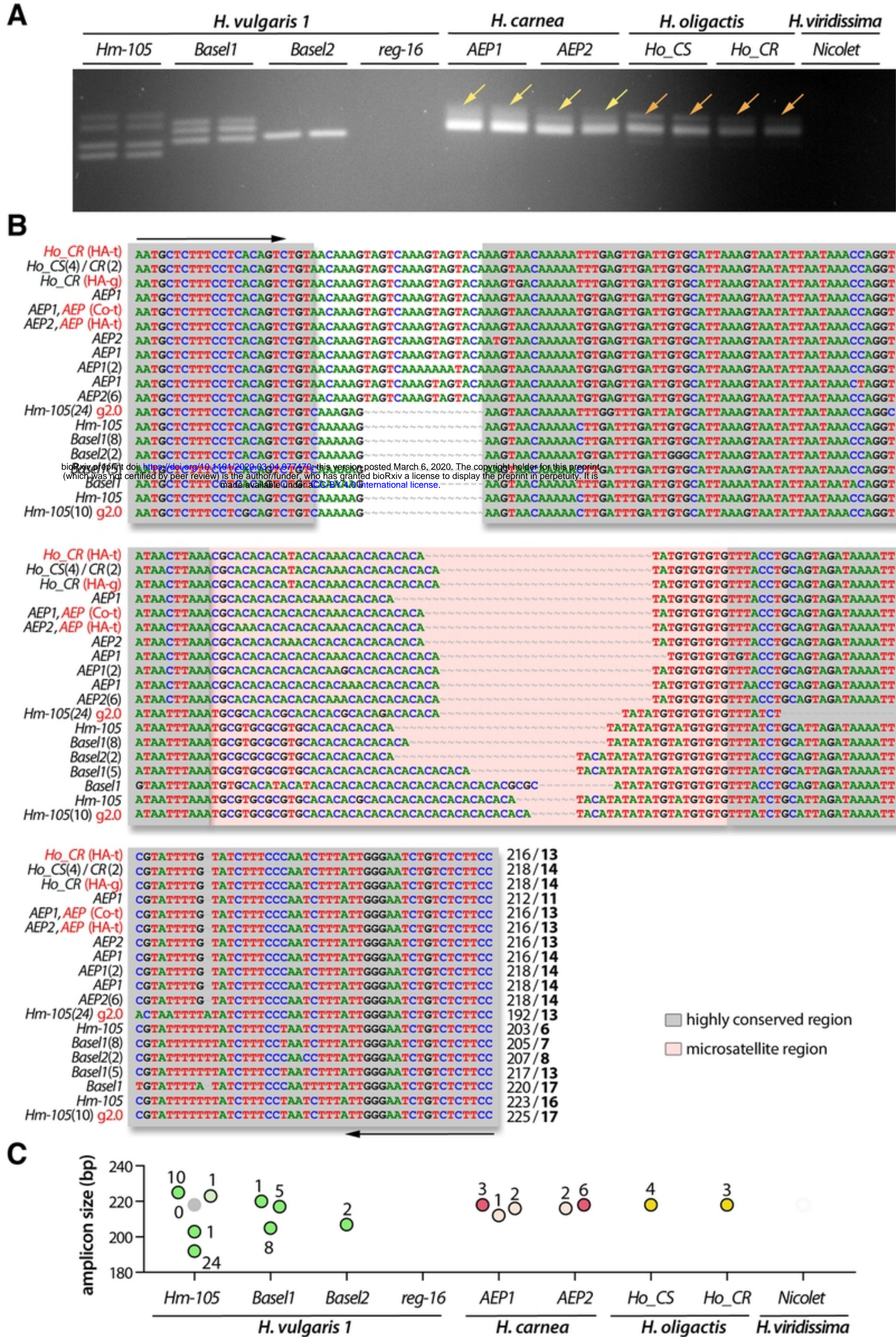


Figure 4

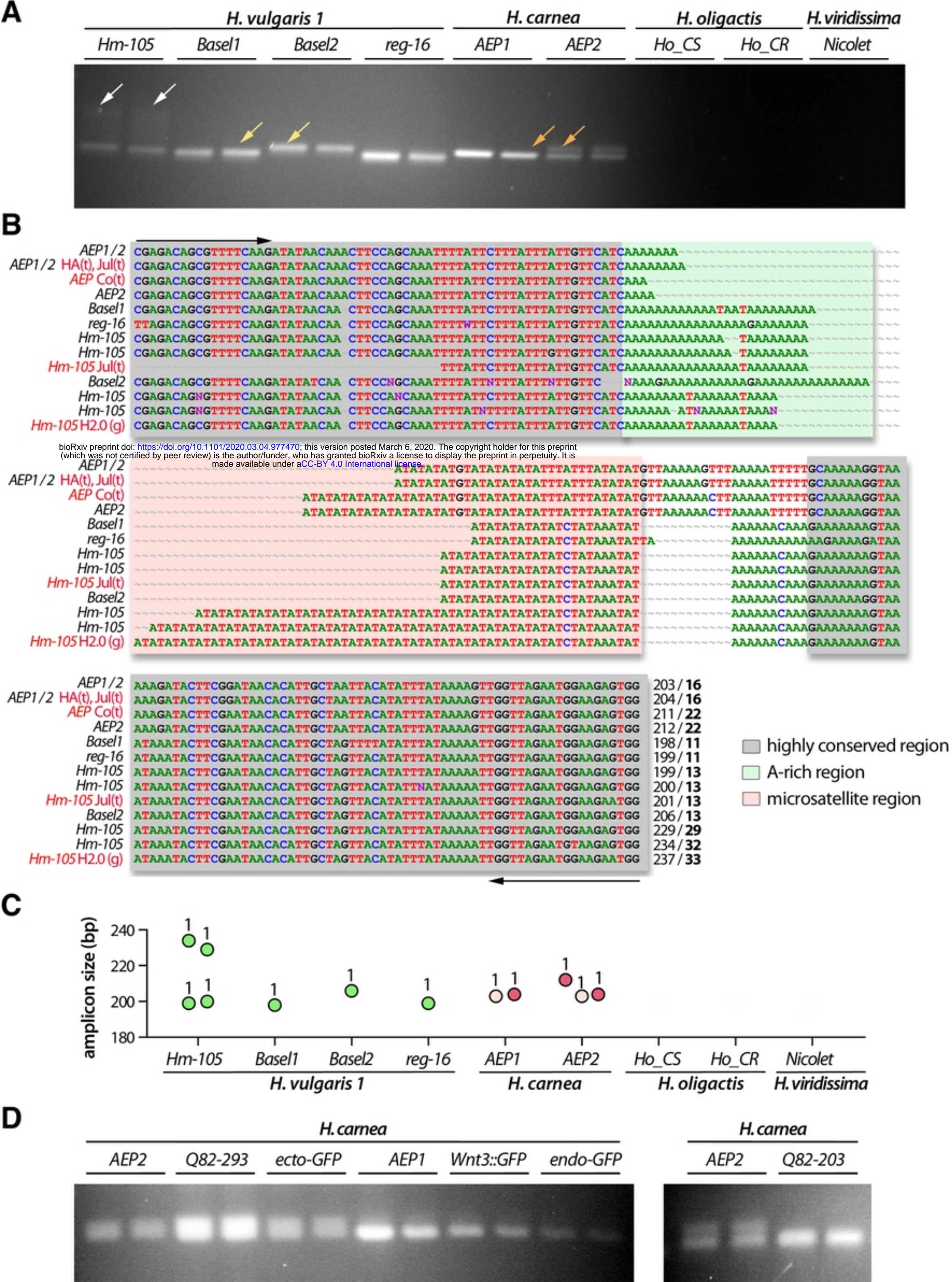


Figure 5

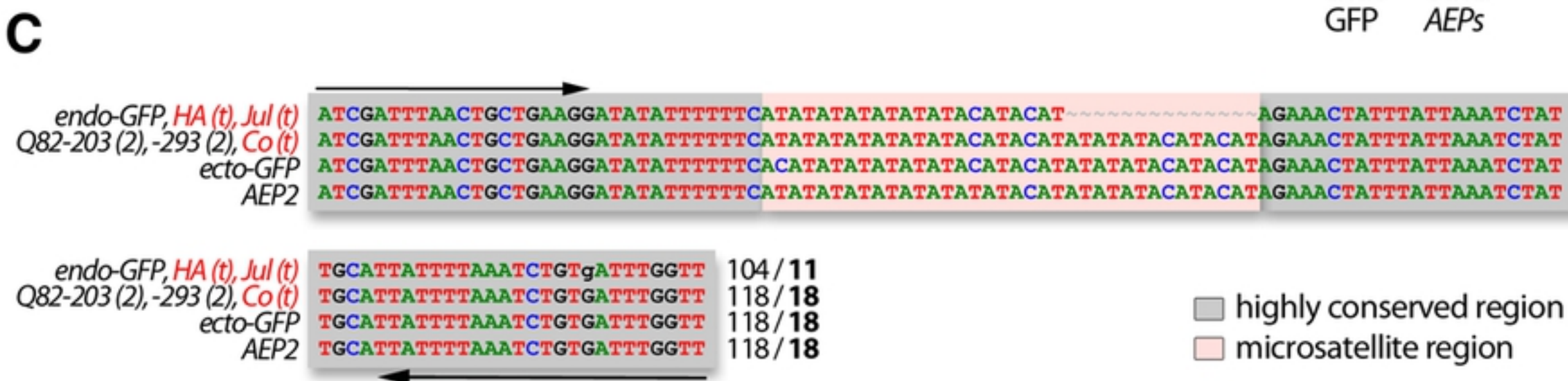
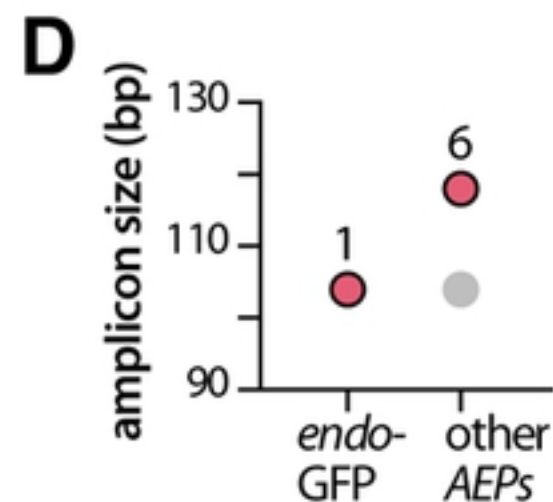
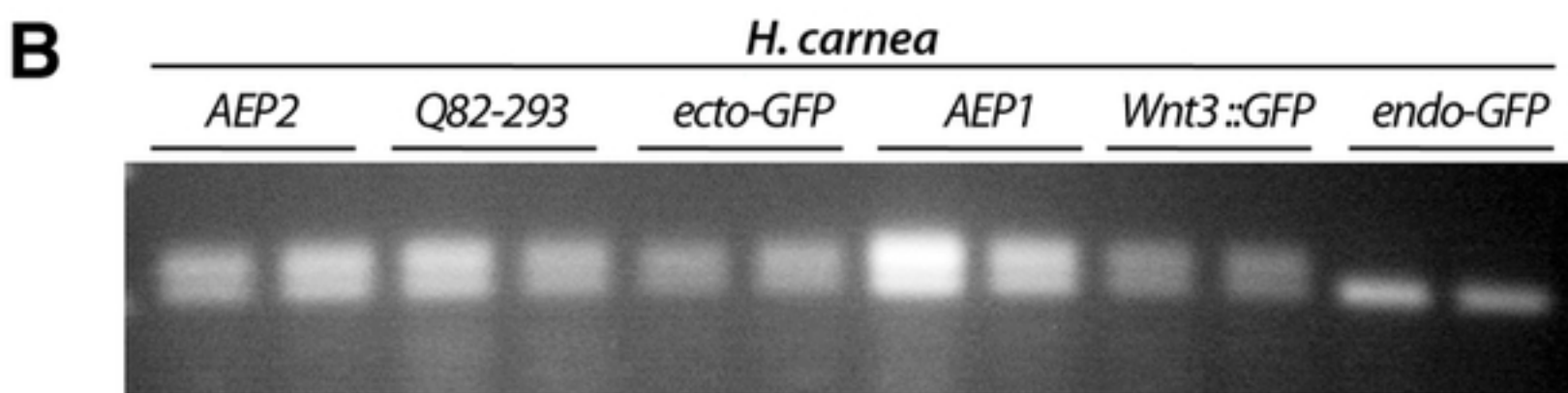
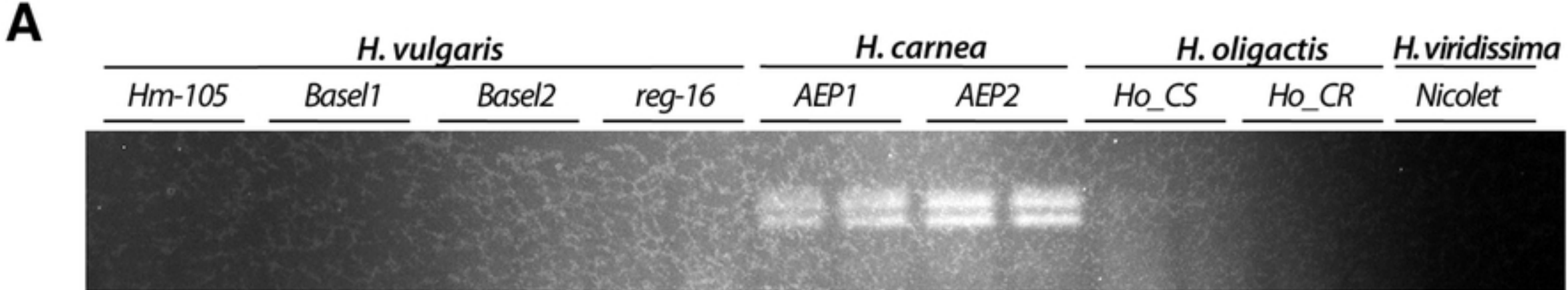


Figure 6

	<i>H. vulgaris</i>												<i>H. carnea</i>						<i>H. oligatis</i>					
	<i>Hm_105</i>			<i>Basel1</i>			<i>Basel2</i>			<i>reg-16</i>			<i>AEP1</i>			<i>AEP2</i>			<i>Ho_CS</i>			<i>Ho_CR</i>		
	<i>ms_c25145</i>	<i>ms_AIP</i>	<i>ms_DMETF1</i>	<i>ms_c25145</i>	<i>ms_AIP</i>	<i>ms_DMETF1</i>	<i>ms_c25145</i>	<i>ms_AIP</i>	<i>ms_DMETF1</i>	<i>ms_c25145</i>	<i>ms_AIP</i>	<i>ms_DMETF1</i>	<i>ms_c25145</i>	<i>ms_AIP</i>	<i>ms_DMETF1</i>	<i>ms_c25145</i>	<i>ms_AIP</i>	<i>ms_DMETF1</i>	<i>ms_c25145</i>	<i>ms_AIP</i>	<i>ms_DMETF1</i>	<i>ms_c25145</i>	<i>ms_AIP</i>	<i>ms_DMETF1</i>
<i>Basel1</i>	√	√	nd																					
<i>Basel2</i>	√	√	nd	√	√	nd																		
<i>reg-16</i>	1/2	√	nd	1/2	=	nd	1/2	√	nd															
<i>AEP1</i>	√	√	1/2	√	=	1/2	√	=	1/2	1/2	√	1/2												
<i>AEP2</i>	√	√	1/2	√	√	1/2	√	√	1/2	1/2	√	1/2	=	√	=									
<i>Ho_CS</i>	√	1/2	nd	√	1/2	nd	√	1/2	nd	1/2	1/2	nd	=	1/2	1/2	=	1/2	1/2						
<i>Ho_CR</i>	√	1/2	nd	√	1/2	nd	√	1/2	nd	1/2	1/2	nd	=	1/2	1/2	=	1/2	1/2	=	nd	nd			
<i>Nicolet</i>	1/2	1/2	nd	1/2	1/2	nd	1/2	1/2	nd	nd	1/2	nd	1/2	1/2	1/2	1/2	1/2	1/2	1/2	1/2	1/2	1/2	nd	nd

- √ microsatellite is informative as distinct patterns between the two strains
- 1/2 microsatellite amplification in only one of the two strains
- = identical microsatellite pattern in the two strains
- nd no amplification of the microsatellite sequences

Figure 7